International Journal of Heat and Mass Transfer 69 (2014) 1–5

Contents lists available at ScienceDirect

International Journal of Heat and Mass Transfer

journal homepage: www.elsevier.com/locate/ijhmt

Technical Note

Study on a BFC-based POD-Galerkin ROM for the steady-state heat transfer problem

Dongxu Han, Bo Yu *, Guojun Yu, Yu Zhao, Wenhua Zhang

National Engineering Laboratory for Pipeline Safety, Beijing Key Laboratory of Urban Oil and Gas Distribution Technology, China University of Petroleum, Beijing 102249, People's Republic of China

ARTICLE INFO

Article history:
Received 22 March 2013
Received in revised form 2 October 2013
Accepted 3 October 2013

Keywords:
Body-fitted coordinates
POD reduced-order model
Steady-state heat transfer
Geometry parameter

ABSTRACT

In this article, a reduced-order model (ROM) is established by the Galerkin projection method based on a body-fitted coordinate (BFC) system. Differing from other proper orthogonal decomposition (POD) based ROMs in relevant literatures, the established model could accurately calculate the physical problems with geometric shapes different from the sample cases. Two typical numerical examples are given to validate this advantage. The results show that the average deviation between the results calculated by the proposed ROM and finite volume method (FVM) is less than 0.06 °C. In addition, the established ROM is proved efficient with the computation speed of the ROM being 128 times and 2749 times faster than that of FVM in the two examples respectively.

1. Introduction

Proper orthogonal decomposition (POD) is a powerful tool for model reduction, and the computation speed can be significantly improved by the application of POD reduced-order model (ROM). Thus this technique has been widely applied in the field of fluid flow and heat transfer.

In the field of fluid flow, Deane et al. [1] calculated POD basis functions from the results of direct numerical simulation and established POD-Galerkin ROMs for transition flows in the grooved pipeline and those around the cylinder respectively. Ravindran [2] applied POD method to the real-time control for the flow past an airfoil. My-Ha et al. [3] employed POD method for optimizing parameters for underwater bubble explosions to generate a desired free surface shape. Fogleman et al. [4] analyzed the flow field information in a combustion engine by POD ROM. Wei Kang et al. [5] proposed a nonlinear POD ROM capable of accurately describing complex fluid dynamical systems.

In the field of heat transfer, Banerjee et al. [6] established a POD-Galerkin ROM for heat transfer in the semi-conductor based on finite element method; Raghupathy et al. [7] established a boundary condition-independent ROM by the combination of POD-Galerkin method and finite volume method; Bialecki et al. [8] discussed the treatment of initial field and boundary condition as well as the error controlling.

To the author's knowledge, the POD based ROMs in relevant references are established for a fixed computational domain, although the boundary conditions, initial fields and property parameters may vary. In engineering, we usually come up with such problems bearing different geometric shapes and sizes but being the same in physics. Establishing a ROM for the flow and heat transfer process of such problems has great value in practical engineering.

Our research group has encountered rapid calculation issues of temperature field of soil surrounding hot oil pipeline with different diameter and buried depth. In reference [9], we employed the BFC-based POD ROM to solve this problem which contains simple configuration and boundary condition.

Based on Ref. [9], a much improved BFC-based POD ROM is presented in this paper. The treatments of Jacobi factor and boundary conditions are quite different in the present study which extends the application range of the POD ROM and simplifies coding.

The paper is organized as follows, the establishment of BFC-based POD reduced-model and treatments of boundary conditions are given firstly, then the accuracy and robustness of the BFC-based reduced-order model is validated by two complex examples.

2. Establishment of the BFC-based POD-Galerkin ROM

The governing equation defined in the BFC for heat conduction problem, transformed from Cartesian coordinate system, is as follows

$$\frac{1}{J}\frac{\partial}{\partial\xi}\left[\frac{\Gamma}{J}\left(\alpha T_\xi-\beta T_\eta\right)\right]+\frac{1}{J}\frac{\partial}{\partial\eta}\left[\frac{\Gamma}{J}\left(\gamma T_\eta-\beta T_\xi\right)\right]+S(\xi,\eta)=0 \tag{1}$$

* Corresponding author. Tel.: +86 10 89733849.
E-mail address: yubobox@vip.163.com (B. Yu).

0017-9310/$ - see front matter © 2013 Elsevier Ltd. All rights reserved.
http://dx.doi.org/10.1016/j.ijheatmasstransfer.2013.10.004

Nomenclature

Roman symbols

T	temperature (°C)
S	physical source term (W/m^3)
a_k	spectrum coefficients
R	residue of the governing equation
q^{ξ}	heat flux on the left and right boundaries of the computation domain (W/m^2)
q^{η}	heat flux on the up and down boundaries of the computation domain (W/m^2)

Greek symbols

Γ	heat conductivity (W/(m^2 °C))
ξ, η	coordinates in a body-fitted coordinate system
α, β, γ, J	geometric parameters in the governing equation
ϕ	basis function
Ω	inner product space

According to the fundamentals of POD, only the first M basis functions are needed to accurately construct the physical field, that is

$$T(\xi,\eta)=\sum_{k=1}^{M}a_k\phi_k(\xi,\eta) \tag{2}$$

Here we define R as the residue of the governing equation

$$R=\frac{\partial}{\partial\xi}\left[\frac{\Gamma}{J}\left(\alpha T_{\xi}-\beta T_{\eta}\right)\right]+\frac{\partial}{\partial\eta}\left[\frac{\Gamma}{J}\left(\gamma T_{\eta}-\beta T_{\xi}\right)\right]+JS(\xi,\eta) \tag{3}$$

In Ref. [9], a special engineering problem without source term is encountered and the Jacobi factor is directly divided out in the establishment process of the ROM. Actually, in establishing more universal reduced-order model, when the residual is defined, Jacobi factor should be put into the source term, otherwise it needs to calculate spatial derivative of Jacobi factor in the ROM which would affect the accuracy of ROM.

Substituting Eq. (2) into Eq. (3) and set the value of the projection to the basis function space as zero, we have

$$\begin{aligned}0=&\left(\frac{\partial}{\partial\xi}\left[\frac{\alpha\Gamma}{J}\frac{\partial\sum_{k=1}^{M}a_k\phi_k(\xi,\eta)}{\partial\xi}-\frac{\beta\Gamma}{J}\frac{\partial\sum_{k=1}^{M}a_k\phi_k(\xi,\eta)}{\partial\eta}\right],\phi_i\right)\\&+\left(\frac{\partial}{\partial\eta}\left[\frac{\gamma\Gamma}{J}\frac{\partial\sum_{k=1}^{M}a_k\phi_k(\xi,\eta)}{\partial\eta}-\frac{\beta\Gamma}{J}\frac{\partial\sum_{k=1}^{M}a_k\phi_k(\xi,\eta)}{\partial\xi}\right],\phi_i\right)\\&+(JS(\xi,\eta),\phi_i)\end{aligned} \tag{4}$$

The first term on the right hand side of the equal sign can be written as below

$$\begin{aligned}&\left(\frac{\partial}{\partial\xi}\left[\frac{\alpha\Gamma}{J}\frac{\partial\sum_{k=1}^{M}a_k\phi_k(\xi,\eta)}{\partial\xi}-\frac{\beta\Gamma}{J}\frac{\partial\sum_{k=1}^{M}a_k\phi_k(\xi,\eta)}{\partial\eta}\right],\phi_i\right)\\&=\sum_{k=1}^{M}a_k\left(\frac{\partial}{\partial\xi}\left(\frac{\alpha\Gamma}{J}\frac{\partial\phi_k(\xi,\eta)}{\partial\xi}-\frac{\beta\Gamma}{J}\frac{\partial\phi_k(\xi,\eta)}{\partial\eta}\right),\phi_i(\xi,\eta)\right)\end{aligned} \tag{5}$$

Applying Green theorem, Eq. (5) could be written as follows

$$\begin{aligned}&\left(\frac{\partial}{\partial\xi}\left[\frac{\alpha\Gamma}{J}\frac{\partial\sum_{k=1}^{M}a_k\phi_k(\xi,\eta)}{\partial\xi}-\frac{\beta\Gamma}{J}\frac{\partial\sum_{k=1}^{M}a_k\phi_k(\xi,\eta)}{\partial\eta}\right],\phi_i\right)\\&=\sum_{k=1}^{M}a_k\oint\left(\frac{\alpha\Gamma}{J}\frac{\partial\phi_k(\xi,\eta)}{\partial\xi}-\frac{\beta\Gamma}{\boldsymbol{J}}\frac{\partial\phi_k(\xi,\eta)}{\partial\eta}\right)\cdot\phi_i(\xi,\eta)d\eta\\&\quad-\sum_{k=1}^{M}a_k\int_{\Omega}\left(\frac{\alpha\Gamma}{J}\frac{\partial\phi_k(\xi,\eta)}{\partial\xi}-\frac{\beta\Gamma}{J}\frac{\partial\phi_k(\xi,\eta)}{\partial\eta}\right)\cdot\frac{\partial\phi_i(\xi,\eta)}{\partial\xi}d\Omega\end{aligned} \tag{6}$$

Similarly, the second term on the right side of the equal sign in Eq. (4) can be expressed by Eq. (7) as below

$$\begin{aligned}&\left(\frac{\partial}{\partial\eta}\left[\frac{\gamma\Gamma}{J}\frac{\partial\sum_{k=1}^{M}a_k\phi_k(\xi,\eta)}{\partial\eta}-\frac{\beta\Gamma}{J}\frac{\partial\sum_{k=1}^{M}a_k\phi_k(\xi,\eta)}{\partial\xi}\right],\phi_i\right)\\&=\sum_{k=1}^{M}a_k\oint\left(\frac{\gamma\Gamma}{J}\frac{\partial\phi_k(\xi,\eta)}{\partial\eta}-\frac{\beta\Gamma}{J}\frac{\partial\phi_k(\xi,\eta)}{\partial\xi}\right)\cdot\phi_i(\xi,\eta)d\xi\\&\quad-\sum_{k=1}^{M}a_k\int_{\Omega}\left(\frac{\gamma\Gamma}{J}\frac{\partial\phi_k(\xi,\eta)}{\partial\eta}-\frac{\beta\Gamma}{J}\frac{\partial\phi_k(\xi,\eta)}{\partial\xi}\right)\cdot\frac{\partial\phi_i(\xi,\eta)}{\partial\eta}d\Omega\end{aligned} \tag{7}$$

And the third term on the right side of the equal sign in Eq. (4) could be described by

$$(JS(\xi,\eta),\phi_i)=\int_{\Omega}JS(\xi,\eta)\cdot\phi_i d\Omega \tag{8}$$

Substituting Eqs. (6)–(8) into Eq. (4), according to the definition of normal derivative on the computation domain, we have

$$\begin{aligned}0=&\oint\Gamma\sqrt{\alpha}\frac{\partial T}{\partial n^{\xi}}\cdot\phi_i(\xi,\eta)d\eta+\oint\Gamma\sqrt{\gamma}\frac{\partial T}{\partial n^{\eta}}\cdot\phi_i(\xi,\eta)d\xi\\&-\sum_{k=1}^{M}a_k\int_{\Omega}\Gamma\sqrt{\alpha}\frac{\partial\phi_k(\xi,\eta)}{\partial n^{\xi}}\cdot\frac{\partial\phi_i(\xi,\eta)}{\partial\xi}d\Omega\\&-\sum_{k=1}^{M}a_k\int_{\Omega}\Gamma\sqrt{\gamma}\frac{\partial\phi_k(\xi,\eta)}{\partial n^{\eta}}\cdot\frac{\partial\phi_i(\xi,\eta)}{\partial\eta}d\Omega+\int_{\Omega}JS(\xi,\eta)\cdot\phi_i(\xi,\eta)d\Omega\end{aligned} \tag{9}$$

According to the definition of heat flux on the boundary, the evolution equation of amplitudes can be obtained as follows

$$0=\sum_{k=1}^{M}H_{ik}a_k+\oint\sqrt{\alpha}q^{\xi}\cdot\phi_i d\eta+\sqrt{\gamma}q^{\eta}\cdot\phi_i d\xi+F_i \tag{10}$$

where $H_{ik}=(\partial\phi_i/\partial\xi,\Gamma\sqrt{\alpha}\partial\phi_k(\xi,\eta)/\partial n^{\xi})+(\partial\phi_i/\partial\eta,\Gamma\sqrt{\gamma}\partial\phi_k(\xi,\eta)/\partial n^{\eta}),F_i=(-JS(\xi,\eta),\phi_i)$.

It can be seen from Eq. (10), the boundary conditions of the physical domain are introduced in the form of heat flux q. Now, the treatment of boundary condition will be clearly introduced by taking the treatment of q^{ξ} for example.

In Ref. [9], three kinds of boundary conditions are dealt with respectively. Here we unify the three kinds of conditions into one expression, the heat flux q^{ξ} on the boundary can be written as

$$q^{\xi}=A\Gamma(\alpha T_{\xi}-\beta T_{\eta})/(J\sqrt{\alpha})+Bq_w+Ch_f(T_f-T(N_0)) \tag{11}$$

where, $A=1$, $B=0$, $C=0$ for the first-type boundary condition; $A=0$, $B=1$, $C=0$ for the second-type boundary condition, and $A=0$, $B=0$, $C=1$ for the third-type boundary condition.

The above equation can be divided into a term without the amplitudes (the first term on the right side of the equal sign in Eqs. (12) and (13) to be solved and a term with the amplitudes (the second term on the right side of the equal sign in Eqs. (12) and (13).

$$
\begin{aligned}
q^{\xi} &= -A\Gamma\beta T_{\eta}/(J\sqrt{\alpha}) + Bq_w + ChT_f - ChT(N_0) \\
&\quad + A\Gamma\sqrt{\alpha}/(Jd)\cdot(T(N_1) - T(N_0)) \\
&= \left[-A\Gamma\beta T_{\eta}/(J\sqrt{\alpha}) + Bq_w + ChT_f - A\Gamma\sqrt{\alpha}/(Jd)\cdot T(N_0)\right] \\
&\quad + \left[-ChT(N_0) + A\Gamma\sqrt{\alpha}/(Jd)\cdot T(N_1)\right] \\
&= \left[-A\Gamma\beta T_{\eta}/(J\sqrt{\alpha}) - A\Gamma\sqrt{\alpha}/(Jd)\cdot T(N_0) + Bq_w + ChT_f\right] \\
&\quad + \left[\sum_{k=1}^{M} a_k(A\Gamma\sqrt{\alpha}/(Jd)\phi_k(N_1) - Ch\phi_k(N_0))\right] \qquad (12)
\end{aligned}
$$

where, N_0 is the identifier of the grid on the boundary, N_1 is the identifier of the inner grid adjacent to the boundary grid N_0, d is the distance between grid N_0 and N_1.

$$
\begin{aligned}
q^{\eta} &= \left[-A\Gamma\beta T_{\xi}/(J\sqrt{\gamma})\cdot -A\Gamma\sqrt{\gamma}/(Jd)\cdot T(N_0) + Bq_w + ChT_f\right] \\
&\quad + \left[\sum_{k=1}^{M} a_k(A\Gamma\sqrt{\gamma}/(Jd)\phi_k(N_1) - Ch\phi_k(N_0))\right] \qquad (13)
\end{aligned}
$$

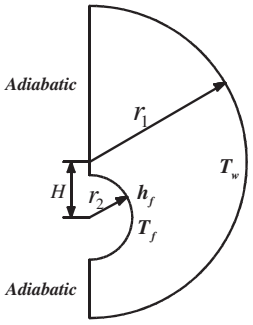

(a) Example 1

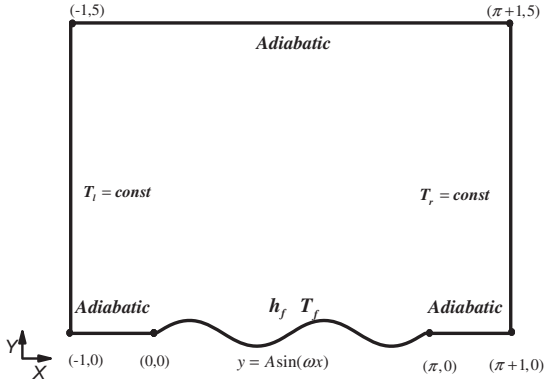

(b) Example 2

Fig. 1. Sketch map of the two validation examples.

Table 1
Computation parameters of the sample cases in Example 1 and Example 2.

Sample cases in Example 1							
Parameter	r_2 m	r_1 m	H m	λ W/(m °C)	h_f W/(m^2 °C)	T^f °C	T^w °C
Value	0.1	0.8	0.1	0.4	5	10	−10
	0.3	1	0.3	1.4	20	30	15
Sample cases in Example 2							
Parameter	A m	ω rad/m	h_f w/(m^2 °C)		λ w/(m °C)	T_f °C	
Value	0.2	1	5		0.4	10	
	0.4	4	20		1.4	30	

Substituting Eqs. (12) and (13) into Eq. (10), the influences of boundary conditions could be introduced into the evolution equation of amplitudes. The amplitudes could be obtained by solving the final evolution equation of amplitudes, and the temperature filed can be constructed by Eq. (2).

3. Numerical examples and results

In this section, two examples, named Examples 1 and 2, are employed to validate the flexibility of the established model. The

Table 2
Computational parameters for validation cases.

Validation cases in Example 1							
Parameter	r_2 m	r_1 m	H m	λ W/(m °C)	h_f W/(m^2 °C)	T^f °C	T^w °C
Within the range	0.15	0.85	0.15	0.8	10	15	0
	0.25	0.95	0.25	1.2	15	20	8
Out of the range	0.4	2	−0.1	5	1	5	−15
	0.8	4	1	10	40	40	30

Validation cases in Example 2					
Parameter Case number	A m	ω rad/m	h_f W/(m^2 °C)	λ W/(m °C)	T_f °C
1	0.3	1	15	3	13
2	0.5	1	15	3	13
3	0.3	2	10	1	8
4	0.2	2	10	1	8
5	0.3	3	3	0.3	10
6	0.3	1	15	3	13
7	0.5	1	15	3	13
8	0.3	2	10	1	8

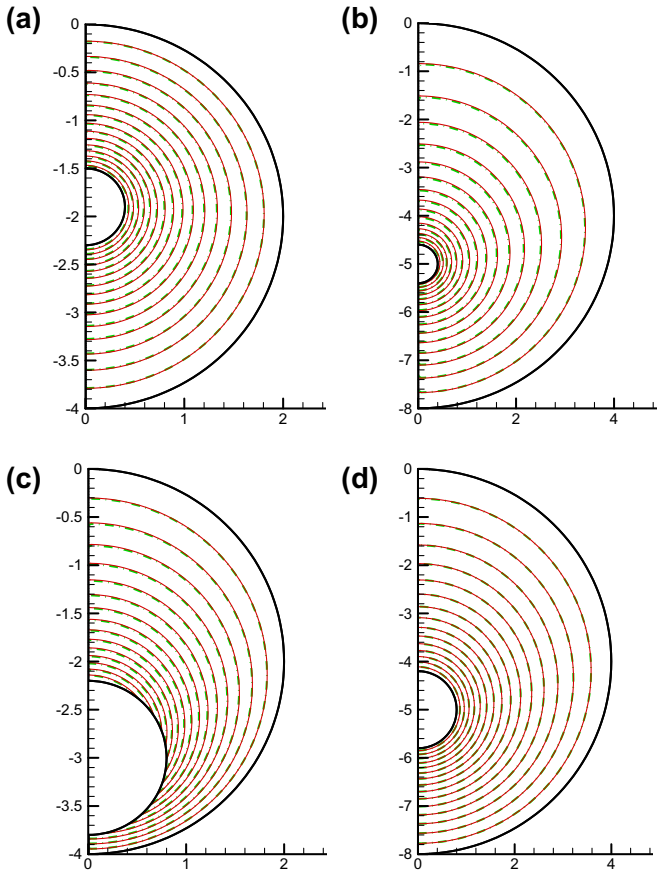

Fig. 2. Comparisons of the results calculated by POD and FVM in Example 1.

physical domains and the boundary conditions can be seen in Fig. 1(a) and (b) respectively.

According to the classic procedures of implementing POD ROM, generating the matrices of the samples is the first step. For the problems which have more variable parameters, sample matrices are usually obtained by overlying different samples bearing different boundary conditions. The computational parameters in Examples 1 and 2 are generated by the permutation and combination of the two values for each parameter in Table 1, which means 128 cases are calculated in Example 1 and 32 cases in Example 2. For Examples 1 and 2, the samples are respectively calculated on the meshes consisting of 80×80 cells and 120×120 cells by FVM using a Gauss–Seidel solver combined with successive over-relaxation (SOR) (the relaxation factor is 1.5) and the convergence criterion is the norm of error lower than 10^{-8}.

By snapshot method, 128 and 32 basis functions are obtained for Examples 1 and 2 respectively from the sampling matrices. Although the first 6 basis functions can capture most of the energy,

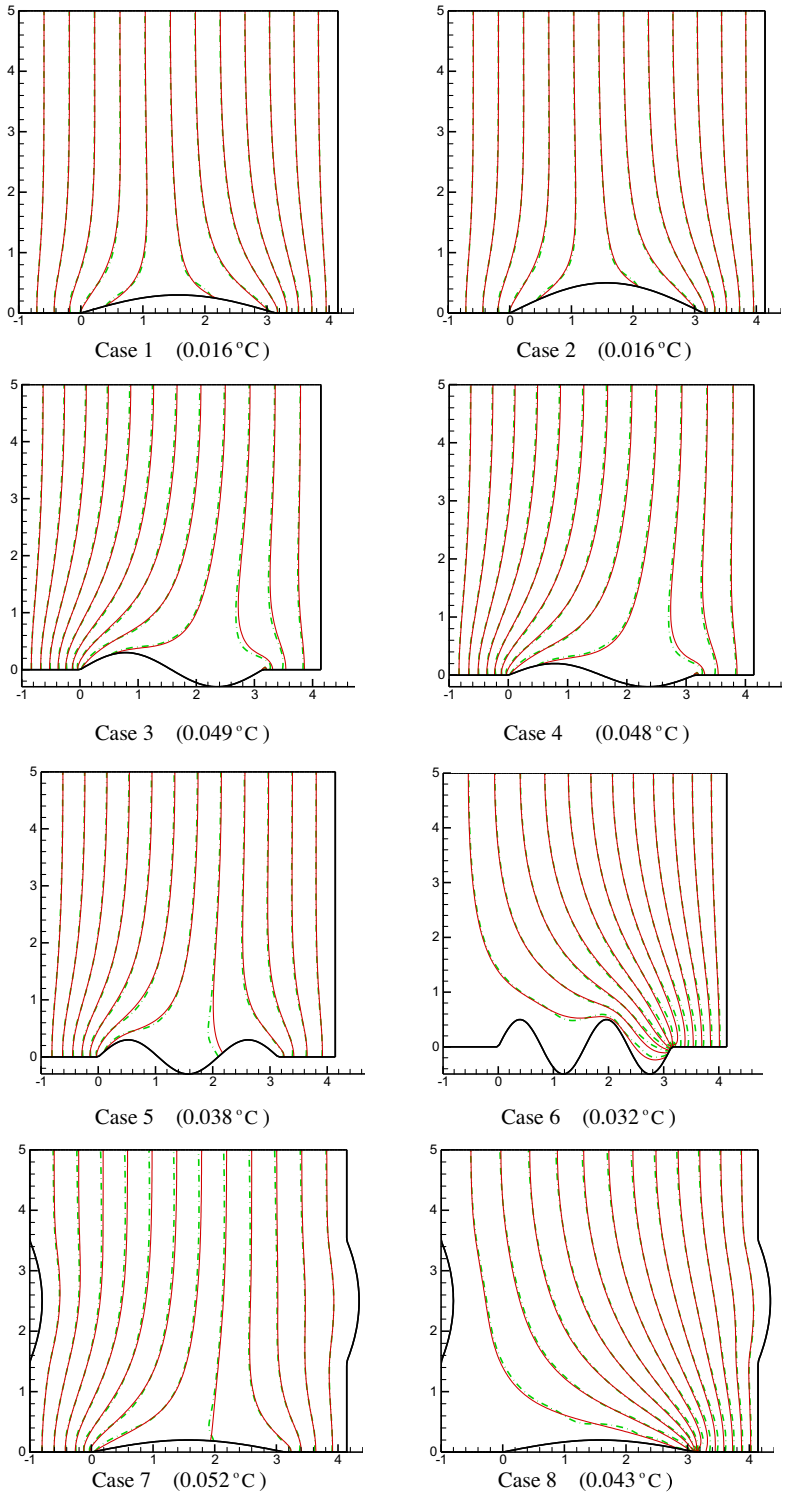

Fig. 3. Comparisons of the results calculated by POD ROM and FVM in Example 2, the values in the brackets are the average errors of POD results.

20 basis functions are required to achieve acceptable accuracy for this two Examples. The reason is that some energy of the basis functions is still located in the areas where the geometric shape sharply changes, although its total energy contribution is very sparse.

After the basis functions are obtained, validation cases are designed. The computational parameters for the validation cases in Examples 1 and 2 are listed in Table 2. Example 1 includes 256 cases, and its computational parameters are determined by the permutation and combination of the two values for each parameter in Table 2. Among the 256 cases, their computational parameters are within the range of sample parameters, while the other half are out of the range of them. For the 8 cases in Example 2, their geometric parameters A and ω are different from those of the sample cases as listed in Table 2, indicating that there is significant difference in geometric shapes between the validation cases and sample cases. In particular, for cases 7 and 8, part of the left boundary in the validation cases is curved, while it is straight in the sample cases.

Fig. 2 presents four typical results of the validation cases in Example 1, which bear different geometric shape from the sample cases. The solid line represents the result achieved by POD ROM, and the dashed line stands for the results calculated by FVM. It can be observed that the proposed ROM is accurate even if there is significant difference in geometric shape between the validation cases and sample cases, and this demonstrates the robustness of the proposed model. It can be obtained the average errors of all the validation cases are very small and limited within the range of 0.0025–0.0325 °C. It is also found that the average errors of the cases containing the parameters out of the range of sample parameters are still lower than 0.0325 °C, even with significant difference in geometric shape between the validation cases and sample cases. To demonstrate the degree to which the present ROM could still provide a reliable solution, typical outer diameter as well as out arc temperature are selected and tests are conducted in a range that is much beyond the sample range. The research results revealed that if the maximum of tolerable average error is set to be 0.01 °C, the value of r_1 could reach 6m and the value of T_w could reach 30 °C which are 6 times and 2 times of the maximum sampling value respectively. While the tolerable average error is set to be 0.02 °C, the value of T_w could be 4 times of the maximum sampling value and the value of r_1 could be 15 times of the maximum sampling value. All this further validates the accuracy and robustness of the proposed BFC-based POD model.

In Fig. 3, the temperature fields gained by the ROM and FVM are compared. The solid line denotes the result by POD ROM, and the dashed line represents that by FVM, and the average deviations are embedded in brackets. It can be seen from Fig. 3 that the results calculated by POD ROM agree well with those by FVM, with the maximum average error lower than 0.06 °C. It is proved that the proposed BFC-based POD ROM is accurate enough even if there is significant difference in geometric shape between the validation cases and sampling cases. And thus the robustness of the model could be validated.

At last, the computation time cost by FVM and the established model are compared Average time of Example 1 cost by FVM and POD are 3.486 and 0.027 s respectively. 318.96 and 0.116 s are respectively consumed by FVM and POD of Example 2. Obviously, the advantage of the ROM is remarkable with its computation speed of the ROM being hundreds times faster than that of FVM, and this advantage would be much more remarkable on a denser mesh.

4. Conclusions

A ROM is established by the Galerkin projection method based on a body-fitted coordinate system. The proposed model has been employed to calculate two heat transfer problems bearing different geometric shapes and sizes with those of sample cases, and the results have been validated to be accurate. The successful application of BFC-based POD ROM to heat transfer problems could be easily extended to other engineering problems which bear different geometric shapes but the same flow and heat transfer process.

Acknowledgement

The study is supported by National Key Projects of Fundamental R/D of China (973 Project: 2011CB610306) and National Science Foundation of China (Nos. 51134006 and 51176204). Dr. Bo YU dedicates this paper to Prof. Wenquan TAO for his 75th birthday.

References

[1] A.E. Deane, I.G. Kevrekidis, G.E. Karniadakis, et al., Low dimensional models for complex geometry flows: application to grooved channels and circular cylinder, Phys. Fluids 3 (1991) 2337–2354.
[2] S.S. Ravindran, Reduced order controllers for control of flow past an airfoil, Int. J. Numer. Methods Fluids 50 (5) (2006) 531–554.
[3] D. My-Ha, K.M. Lim, B.C. Khoo, et al., Real time optimization using proper orthogonal decomposition: free surface shape prediction due to underwater bubble dynamics, Comput. Fluids 36 (3) (2006) 499–512.
[4] M. Fogleman, J. Lumle, D. Rempfer, et al., Application of the proper orthogonal decomposition to datasets of internal combustion engine flows, J. Turbul. 5 (2004) 1–18.
[5] W. Kang, J.Z. Zhang, K.L. Li, Nonlinear Galerkin method for dimension reduction using proper orthogonal decomposition, J. Xi'an Jiaotong Univ. 45 (11) (2011) 58–62.
[6] S. Banerjee, J.V. Cole, K.F. Jensen, Nonlinear model reduction strategies for rapid thermal processing systems, IEEE Trans. Semicond. Manuf. 11 (2) (1998) 266–275.
[7] A.P. Raghupathy, U. Ghia, K. Ghia, Boundary-condition-independent ROMing of complex 2D objects by POD-Galerkin methodology, in: Semiconductor Thermal Measurement and Management Symposium: Proceedings of 25th IEEE Semitherm, 2009, 208–215.
[8] R.A. Bialecki, A.J. Kassab, A. Fic, Proper orthogonal decomposition and modal analysis for acceleration of transient FEM thermal analysis, Int. J. Numer. Methods Eng. 62 (6) (2005) 774–794.
[9] B. Yu, G. Yu, Z. Cao, D. Han, Q. Shao, Fast calculation of the soil temperature field around a buried oil pipeline using a body-fitted coordinates-based POD Galerkin ROM, Numer. Heat Transfer A: Appl. 63 (10) (2013) 776–794.